Available online at www.sciencedirect.com
SCIENCE DIRECT®
Journal of Sound and Vibration 281 (2005) 699–717
JOURNAL OF SOUND AND VIBRATION
www.elsevier.com/locate/jsvi

Airfoil motion in subsonic flow with strong cubic nonlinear restoring forces

B.H.K. Lee[a,*], L. Liu[b], K.W. Chung[c]

[a]*Aerodynamics Laboratory, National Research Council, Institute for Aerospace Research, Ottawa, Ontario, Canada K1A 0R6*
[b]*Department of Mechanical Engineering and Materials Science, Duke University, Durham, NC 27708, USA*
[c]*Deptartment of Mathematics, City University, Hong Kong, China*

Received 25 August 2003; accepted 30 January 2004

Abstract

Limit cycle oscillations of a two-degree-of-freedom airfoil motion with cubic nonlinearity in the restoring forces are investigated. The harmonic balance method is used to derive a frequency relation that depends only on airfoil parameters. The amplitudes of the pitch and plunge motions can be computed from analytical expressions once the frequency is known. The method is extended to higher harmonics. Illustrative examples are given and the results are compared with numerical computations.

1. Introduction

The motion of an airfoil with a cubic nonlinearity in the stiffness restoring force has been studied as early as the 1950s by Woolston et al. [1] and Shen [2]. This problem was later analysed numerically by Lee and LeBlanc [3], and analytically by Lee et al. [4] and Liu et al. [5]. Experimentally, O'Neil and Stragnac [6] investigated the flutter boundary for limit cycle oscillations and found the agreement with numerical simulation to be fairly satisfactory. The theoretical studies were mainly concerned with cubic nonlinearities that are small. For small

*Corresponding author. Tel.: +1-613-998-3401; fax: +1-613-998-1281.
E-mail address: ben.lee@nrc-cnrc.gc.ca (B.H.K. Lee).

0022-460X/$ - see front matter © 2004 Elsevier Ltd. All rights reserved.
doi:10.1016/j.jsv.2004.01.034

Nomenclature

a_h	non-dimensional distance from airfoil mid-chord to elastic axis
b	airfoil semi-chord
C_h, C_a	damping coefficients in plunge and in pitch
$C_L(\tau)$, $C_M(\tau)$	aerodynamic lift and pitching moment coefficients
f	non-dimensional linear frequency
$G(\xi)$, $M(\alpha)$	nonlinear plunge and pitch stiffness terms
HB1	first harmonic balance method
HB3	third harmonic balance method
h	plunge displacement
I_a	airfoil mass moment of inertia about elastic axis
K_ξ, K_α	stiffness in plunge and in pitch, $K_\xi = K_h$
m	airfoil mass
$P(\tau)$	externally applied forces
$p(t)$	forces acting on the airfoil
$Q(\tau)$	externally applied moments
R_1, R_3	amplitudes of the first and the third harmonics in the pitch motion
$r(t)$	moments acting on the airfoil
r_a	radius of gyration about the elastic axis
S	airfoil static moment about the elastic axis
t	time
U	free-stream velocity
U^*	non-dimensional velocity, $U^* = U/(b\omega_\alpha)$.
U_L^*	linear flutter speed
$\mathbf{X}$	eight-dimensional vector variable
x_a	non-dimensional distance from the airfoil elastic axis to the centre of mass
α	pitch angle of airfoil
β	cubic coefficient in pitch
γ	cubic coefficient in plunge
ε_1, ε_2	constants in Wagner's function
ζ_a, ζ_ξ	viscous damping ratios in pitch and in plunge
μ	airfoil/air mass ratio, $\mu = m/(\pi\rho b^2)$
ξ	nondimensional plunge displacement, $\xi = h/b$.
τ	non-dimensional time, $\tau = Ut/b$
$\phi(\tau)$	Wagner's function
ϕ_3	phase angle in the pitch motion
φ_1, φ_3	phase angles in the plunge motion
ψ_1, ψ_2	constants in Wagner's function
ω	fundamental frequency of the motion
ω_ξ, ω_α	natural frequencies in plunge and in pitch
$\bar{\omega}$	frequency ratio, $\bar{\omega} = \omega_\xi/\omega_\alpha$

departure from linearity for the structural stiffness, it was found in Ref. [4] that at a velocity U^* equal to the linear flutter speed U_L^*, a supercritical Hopf bifurcation emerges and limit cycle oscillations are observed at increasing U^*/U_L^* ratios above unity. However, when large nonlinear structural forces are present, the airfoil motion may exhibit other types of motion.

This paper considers only structural nonlinearities although in aeroelastic problems aerodynamic nonlinearities are also important at high subsonic velocities, especially at transonic flow conditions [7]. Recently, Thomas et al. [8] used a frequency domain harmonic balance method to model limit cycle oscillations of airfoil sections.

2. Analytical formulation

Fig. 1 gives the symbols used in the analysis of a two-degree-of-freedom (2-dof) airfoil motion. The plunge deflection is denoted by h, positive in the downward direction, and α is the pitch angle

about the elastic axis, positive nose up. The elastic axis is located at a distance $a_h b$ from the mid-chord, while the mass centre is located at a distance $x_a b$ from the elastic axis, where b is the airfoil semi-chord. Both distances are positive when measured towards the trailing edge of the airfoil. The aeroelastic equations of motion for linear springs have been derived by Fung [9]. For nonlinear restoring forces, the coupled bending-torsion equations for the airfoil can be written as follows:

$$m\ddot{h} + S\ddot{\alpha} + C_h\dot{h} + \bar{G}(h) = p(t), \tag{1}$$

$$S\ddot{h} + I_\alpha\ddot{\alpha} + C_\alpha\dot{\alpha} + \bar{M}(\alpha) = r(t), \tag{2}$$

where the symbols m, S, C_h, I_α and C_α are the airfoil mass, airfoil static moment about the elastic axis, damping coefficient in plunge, wing mass moment of inertia about elastic axis, and torsion damping coefficient, respectively. $\bar{G}(h)$ and $\bar{M}(\alpha)$ are the nonlinear plunge and pitch stiffness terms, and $p(t)$ and $r(t)$ are the forces and moments acting on the airfoil, respectively. Defining $\xi = h/b$, $K_\xi = K_h$, $x_\alpha = S/bm$, $\omega_\xi = (K_\xi/m)^{1/2}$, $\omega_\alpha = (K_\alpha/I_\alpha)^{1/2}$, $r_\alpha = (I_\alpha/mb^2)^{1/2}$, $\zeta_\xi = C/2(mK_h)^{1/2}$ and $\zeta_\alpha = C/2(I_\alpha K_\alpha)^{1/2}$, Eqs. (1) and (2) can be written in nondimensional form [7] as follows:

$$\xi'' + x_\alpha\alpha'' + 2\zeta_\xi\frac{\bar{\omega}}{U^*}\xi' + \left(\frac{\bar{\omega}}{U^*}\right)^2 G(\xi) = -\frac{1}{\pi\mu}C_L(\tau) + \frac{P(\tau)b}{mU^2}, \tag{3}$$

$$\frac{x_\alpha}{r_\alpha^2}\xi'' + \alpha'' + 2\frac{\zeta_\alpha}{U^*}\alpha' + \frac{1}{U^{*2}}M(\alpha) = \frac{2}{\pi\mu r_\alpha^2}C_M(\tau) + \frac{Q(\tau)}{mU^2r_\alpha^2}, \tag{4}$$

where $G(\xi) = \bar{G}(h)/K_\xi$ and $M(\alpha) = \bar{M}(\alpha)/K_\alpha$.

In Eqs. (3) and (4), U^* is a nondimensional velocity defined as $U^* = U/b\,\omega_\alpha$ and $\bar{\omega} = \omega_\xi/\omega_\alpha$, where ω_ξ and ω_α are the uncoupled plunging and pitching mode natural frequencies, respectively, U is the freestream velocity, and the $'$ denotes differentiation with respect to the nondimensional time τ defined as $\tau = Ut/b$. $C_L(\tau)$ and $C_M(\tau)$ are the lift and pitching moment coefficients, respectively, and μ is the airfoil/air mass ratio $(m/\pi\rho^2)$. For incompressible flow, Fung [9] gives the

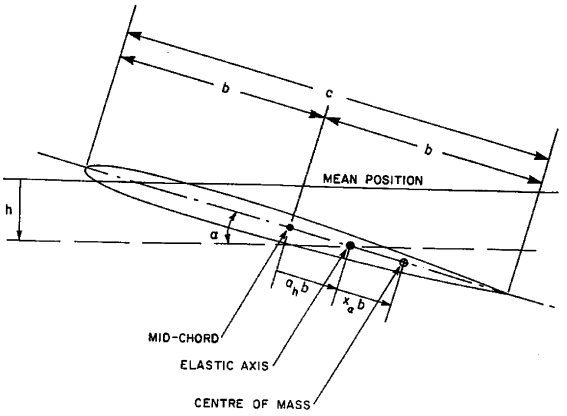

Fig. 1. Schematic of airfoil with 2 dof motion.

following expressions for $C_L(\tau)$ and $C_M(\tau)$:

$$C_L(\tau) = \pi\left(\xi'' - a_h\alpha'' + \alpha'\right) + 2\pi\left\{\alpha(0) + \xi'(0) + \left[\tfrac{1}{2} - a_h\right]\alpha'(0)\right\}\phi(\tau) + 2\pi\int_0^\tau \phi(\tau-\sigma)\left[\alpha'(\sigma) + \xi''(\sigma) + \left(\tfrac{1}{2} - a_h\right)\alpha''(\sigma)\right] d\sigma, \tag{5}$$

$$C_M(\tau) = \pi\left(\tfrac{1}{2} + a_h\right)\left\{\alpha(0) + \xi'(0) + \left(\tfrac{1}{2} - a_h\right)\alpha'(0)\right\}\phi(\tau) + \pi\left(\tfrac{1}{2} + a_h\right)\int_0^\tau \phi(\tau-\sigma)\left\{\alpha'(\sigma) + \xi''(\sigma) + \left(\tfrac{1}{2} - a_h\right)\alpha''(\sigma)\right\} d\sigma + \frac{\pi}{2}a_h\left(\xi'' - a_h\alpha''\right) - \left(\tfrac{1}{2} - a_h\right)\frac{\pi}{2}\alpha' - \frac{\pi}{16}\alpha'', \tag{6}$$

where the Wagner function $\phi(\tau)$ is given by

$$\phi(\tau) = 1 - \psi_1 e^{-\varepsilon_1\tau} - \psi_2 e^{-\varepsilon_2\tau} \tag{7}$$

and the constants $\psi_1 = 0.165$, $\psi_2 = 0.335$, $\varepsilon_1 = 0.0455$ and $\varepsilon_2 = 0.3$ are obtained from Jones [10]. $P(\tau)$ and $Q(\tau)$ are the externally applied forces and moments, respectively, and they are set to zero in this study.

Due to the presence of the integral terms in the integro-differential equations. (3) and (4), it is cumbersome to integrate them numerically. A set of simpler equations was derived by Lee et al. [7], and they introduced four new variables

$$w_1 = \int_0^\tau e^{-\varepsilon_1(\tau-\sigma)}\alpha(\sigma)\, d\sigma, \quad w_2 = \int_0^\tau e^{-\varepsilon_2(\tau-\sigma)}\alpha(\sigma) d\sigma,$$
$$w_3 = \int_0^\tau e^{-\varepsilon_1(\tau-\sigma)}\xi(\sigma)\, d\sigma, \quad w_4 = \int_0^\tau e^{-\varepsilon_2(\tau-\sigma)}\xi(\sigma)\, d\sigma. \tag{8}$$

The resulting set of eight first-order ordinary differential equations by a suitable transformation is given as

$$d\mathbf{X}/d\tau = \mathbf{f}(\mathbf{X}, \tau) \tag{9}$$

where $\mathbf{X} = \{x_1, x_2, ..., x_8\} = \left\{\alpha, \alpha', \xi, \xi', w_1, w_2, w_3, w_4\right\} \in \mathbf{R}^8$.

For a cubic spring in the pitch dof, $M(\alpha)$ is given by

$$M(\alpha) = \alpha + \beta\alpha^3, \tag{10}$$

where β is a constant. When $\beta > 0$, $M(\alpha)$ represents a cubic hard spring while it represents a cubic soft spring when $\beta < 0$. For a cubic spring in the plunge dof, similar to Eq. (10), $G(\xi)$ is given by

$$G(\xi) = \xi + \gamma\xi^3, \tag{11}$$

where γ is a constant. Hence, the aeroelastic system for a self-excited system with cubic nonlinearities of the form given in Eqs. (10) and (11) can be written as

$$\begin{aligned} &c_0\xi'' + c_1\alpha'' + c_2\xi' + c_3\alpha' + (c_4 + c_{10})\xi + c_5\alpha + c_6 w_1 \\ &\quad + c_7 w_2 + c_8 w_3 + c_9 w_4 + c_{10}\gamma\xi^3 = 0, \\ &d_0\xi'' + d_1\alpha'' + d_2\xi' + d_3\alpha' + d_4\xi + (d_5 + d_{10})\alpha + d_6 w_1 \\ &\quad + d_7 w_2 + d_8 w_3 + d_9 w_4 + d_{10}\beta\alpha^3 = 0. \end{aligned} \tag{12}$$

The coefficients c_i and d_i ($i=0,1,2,\ldots,10$) are functions of system parameters and the expressions are given in Appendix A.

2.1. First harmonic balance method

First, we study a single cubic hard spring in the pitch dof, i.e. $\beta \neq 0$ and $\gamma = 0$. For motions dominated by the first harmonic, we assume [2]

$$\alpha(\tau) = a_1 \sin \omega\tau, \quad \xi(\tau) = e_1 \sin \omega\tau + f_1 \cos \omega\tau. \tag{13}$$

Substituting Eq. (13) into Eqs. (8) and (12), and collecting the coefficients of $\sin \omega\tau$ and $\cos \omega\tau$, we obtain the system of a_1, e_1, f_1 and ω:

$$\begin{aligned} &m_1 a_1 + p_1 e_1 + q_1 f_1 = 0, \quad m_2 a_1 + p_2 e_1 + q_2 f_1 = 0, \\ &m_3 a_1 + p_3 e_1 + q_3 f_1 + \tfrac{3}{4} d_{10} \beta a_1^3 = 0, \quad m_4 a_1 + p_4 e_1 + q_4 f_1 = 0, \end{aligned} \tag{14}$$

where m_i ($i=1, 2, 3, 4$), p_i ($i=1, 2, 3, 4$), and q_i ($i=1, 2, 3, 4$) are functions of system parameters and frequency ω , and their expressions are given in Appendix B. For velocities larger than the bifurcation value, the motions have limited-amplitude, i.e. there exist nonzero solutions to Eq. (14). The first, second and fourth equations of Eq. (14) are linear in a_1, e_1 and f_1. Therefore, the determinant of these three equations should be zero, i.e. the frequency of the motion satisfies the algebraic equation

$$m_1(p_2 q_4 - p_4 q_2) - m_2(p_1 q_4 - p_4 q_1) + m_4(p_1 q_2 - p_2 q_1) = 0. \tag{15}$$

This equation can be converted to a polynomial equation. Writing $x = \omega^2$, we have after some algebra the following frequency equation (in terms of x, t_1 and t_2):

$$L_0 + L_1 t_1 + L_2 t_2 + L_3 t_1^2 + L_4 t_2^2 + L_5 t_1 t_2 + L_6 t_1^3 + L_7 t_2^3 + L_8 t_1^2 t_2 + L_9 t_1 t_2^2 = 0. \tag{16}$$

L_i ($i = 0,\ldots,9$) are given in Appendix C. For the cases we shall consider (see the next section) where $a_h = -1/2$, Eq. (16) can be simplified since $L_i = 0$ ($i=6,7,8,9$), and it can be expressed as

$$\begin{aligned} &(\varepsilon_1^2 + x)^2(\varepsilon_2^2 + x)^2 L_0 + (\varepsilon_1^2 + x)(\varepsilon_2^2 + x)^2 L_1 + (\varepsilon_1^2 + x)^2(\varepsilon_2^2 + x) L_2 \\ &+ (\varepsilon_2^2 + x)^2 L_3 + (\varepsilon_1^2 + x)^2 L_4 + (\varepsilon_1^2 + x)(\varepsilon_2^2 + x) L_5 = 0. \end{aligned} \tag{17}$$

Eq. (17) is a six-degree polynomial equation in x, and the highest order of x is in the first term since L_i ($i=0,1,2,\ldots,5$) are quadratic polynomials of x.

If the condition $L_i = 0$ ($i=6,7,8,9$) is not satisfied, Eq. (16) yields an eight-degree polynomial equation in x, similar to Eq. (17). Once the frequency is obtained, e_1 and f_1 can be solved from the first two equations of Eq. (14) in terms of a_1, that is,

$$e_1 = E_1 a_1, \qquad f_1 = F_1 a_1, \tag{18}$$

where E_1 and F_1 are functions of system parameters and the frequency ω, and their expressions are given in Appendix B. Substituting Eq. (18) into the third equation of Eq. (14) yields the

solution of a_1 as

$$a_1 = \sqrt{-\frac{4(m_3 + p_3E_1 + q_3F_1)}{3d_{10}\beta}}. \tag{19}$$

Since a_1 is the amplitude of the pitch motion, Eq. (19) is the amplitude–frequency relationship for the pitch motion. From Eqs. (18) and (19) the amplitude–frequency relation for the plunge motion is given as

$$r_1 = \sqrt{e_1^2 + f_1^2} = \sqrt{-\frac{4\left(E_1^2 + F_1^2\right)(m_3 + p_3E_1 + q_3F_1)}{3d_{10}\beta}}. \tag{20}$$

Therefore, given a set of system parameters, first the frequency can be solved from Eq. (16) or (17) if $L_i = 0$ ($i = 6,\ldots,9$), then the amplitude of the pitch and plunge motions can be calculated from Eqs. (19) and (20). Taking the pitch motion as reference, the phase shift between the pitch and plunge motion can be calculated from

$$\varphi_1 = \arctan\frac{m_1p_2 - m_2p_1}{-m_1q_2 + m_2q_1}. \tag{21}$$

The results obtained from Eqs. (16)–(21) are the same as those from Lee et al. [7] but the approach given herein is easier to use since no iteration for the amplitude of the airfoil motion is required. Similar expressions can be obtained for the plunge dof with $\beta = 0$ and $\gamma \neq 0$. For nonlinearities in both dof's, i.e. $\beta \neq 0$ and $\gamma \neq 0$, Eq. (13) gives the relationship between a_1, e_1, f_1 and ω as follows:

$$\begin{aligned} &m_1a_1 + p_1e_1 - p_2f_1 + \tfrac{3}{4}c_{10}\gamma e_1r_1^2 = 0, \quad m_2a_1 + p_2e_1 + p_1f_1 + \tfrac{3}{4}c_{10}\gamma f_1r_1^2 = 0,\\ &m_3a_1 + p_3e_1 - p_4f_1 + \tfrac{3}{4}d_{10}\beta a_1r_1^2 = 0, \quad m_4a_1 + p_4e_1 + p_3f_1 = 0. \end{aligned} \tag{22}$$

Eq. (22) can be solved using the Maple [11] program with a defined initial range for the frequency. However, an analytical solution of the frequency similar to Eq. (15) has not yet been successfully derived.

2.2. Higher harmonic balance method

Including terms with 2ω in Eq. (13), and after carrying out similar analysis as outlined above, we can show for the airfoil parameters used in this study that the pitch and plunge amplitudes are zero. The second dominant harmonic is associated with a frequency of 3ω. For a higher order approximation in the analytical prediction, we write Eq. (13) as follows:

$$\begin{aligned} \alpha(\tau) &= a_1\sin\omega\tau + a_3\sin 3\omega\tau + b_3\cos 3\omega\tau,\\ \xi(\tau) &= e_1\sin\omega\tau + f_1\cos\omega\tau + e_3\sin 3\omega\tau + f_3\cos 3\omega\tau. \end{aligned} \tag{23}$$

Substituting Eq. (23) into Eqs. (7) and (12), and upon collecting the coefficients of $\sin\omega\tau$, $\cos\omega\tau$, $\sin 3\omega\tau$ and $\cos 3\omega\tau$, we obtain the system of a_1, e_1, f_1, ω, a_3, b_3, e_3 and f_3

as follows:

$$m_1a_1 + p_1e_1 + q_1f_1 = 0, \quad m_2a_1 + p_2e_1 + q_2f_1 = 0$$
$$m_3a_1 + p_3e_1 + q_3f_1 + d_{10}\beta\left(-\tfrac{3}{4}R_1^2a_3 + \tfrac{3}{4}R_1^2a_1 + \tfrac{3}{2}R_3^2a_1\right) = 0,$$
$$m_4a_1 + p_4e_1 + q_4f_1 + d_{10}\beta\left(-\tfrac{3}{4}R_1^2b_3\right) = 0, \tag{24}$$

$$m_{13}a_3 + n_{13}b_3 + p_{13}e_3 + q_{13}f_3 = 0, \quad m_{23}a_3 + n_{23}b_3 + p_{23}e_3 + q_{23}f_3 = 0$$
$$m_{33}a_3 + n_{33}b_3 + p_{33}e_3 + q_{33}f_3 + d_{10}\beta\left(\tfrac{3}{4}R_3^2a_3 + \tfrac{3}{2}R_1^2a_3 - \tfrac{1}{4}R_1^2a_1\right) = 0,$$
$$m_{43}a_3 + n_{43}b_3 + p_{43}e_3 + q_{43}f_3 + d_{10}\beta\left(\tfrac{3}{4}R_3^2b_3 + \tfrac{3}{2}R_1^2b_3\right) = 0,$$

where $R_1^2 = a_1^2$ and $R_3^2 = a_3^2 + b_3^2$. The expressions for m_i ($i=1,2,3,4$), p_i ($i=1,2,3,4$) and q_i ($i=1,2,3,4$) are given in Appendix B, and the expressions for m_{i3} ($i=1,2,3,4$), n_{i3} ($i=1,2,3,4$), p_{i3} ($i=1,2,3,4$) and q_{i3} ($i=1,2,3,4$) are given in Appendix D. The variables e_1 and f_1 in terms of a_1 can be solved from the first two expressions in (24), and their solutions are the same as Eq. (18). The variables e_3 and f_3 can be solved from the fifth and sixth expressions in (24) in terms of a_3 and b_3 as

$$e_3 = E_3a_3 - F_3b_3\,, \quad f_3 = F_3a_3 + E_3b_3, \tag{25}$$

where E_3 and F_3 are given in Appendix D. Substituting Eqs. (18) and (25) into the other four expressions in (24), we obtain a system of four equations in a_1, a_3, b_3, and ω:

$$M_3a_1 + d_{10}\beta\left(-\tfrac{3}{4}R_1^2a_3 + \tfrac{3}{4}R_1^2a_1 + \tfrac{3}{2}R_3^2a_1\right) = 0, \quad M_4a_1 - d_{10}\beta\tfrac{3}{4}R_1^2b_3 = 0,$$
$$M_{33}a_3 + N_{33}b_3 + d_{10}\beta(\tfrac{3}{4}R_3^2a_3 + \tfrac{3}{2}R_1^2a_3 - \tfrac{1}{4}R_1^2a_1) = 0,$$
$$M_{43}a_3 + N_{43}b_3 + d_{10}\beta(\tfrac{3}{4}R_3^2b_3 + \tfrac{3}{2}R_1^2b_3) = 0, \tag{26}$$

where M_3, M_4, M_{33}, M_{43}, N_{33}, and N_{43} are functions of system parameters and the fundamental frequency ω, and they are given in Appendix D. Using the relationships between n_{i3} and m_{i3}, and q_{i3} and p_{i3} ($i=1,2,3,4$) in Appendix D, we have $N_{43} = M_{33}$ and $M_{43} = -N_{33}$.

After some algebraic manipulations we obtain the frequency relation

$$\begin{aligned} &M_4^5 - 8M_4^4M_{43} + M_4^3(10M_{43}^2 + 4M_{33}^2 + M_3^2 - 4M_{33}M_3) \\ &+ M_4^2(30M_{43}M_{33}M_3 - 9M_{43}M_{33}^2 - 12M_{43}M_3^2 - 24M_{43}^2) \\ &+ M_4(36M_{43}^2M_3^2 - 30M_{43}^2M_{33}M_3 + 9M_{43}^4 + 9M_{43}^2M_{33}^2) \\ &+ 3M_{43}^3M_3^2 = 0. \end{aligned} \tag{27}$$

Eq. (27) can be converted to a polynomial of x with degree of 37, where $x = \omega^2$. Four roots are positive, and the others are negative, zero or complex.

After considerable algebraic manipulations, R_1^2 and R_3^2 can be obtained as follows:

$$R_1^2 = \frac{1}{d_{10}\beta}\frac{4M_{43}(M_3M_{43} + M_4M_{33})}{M_4^2 - 4M_4M_{43} - 3M_{43}^2}, \tag{28}$$

$$R_3^2 = \frac{1}{d_{10}\beta}\frac{4M_4(M_3M_4 + M_4M_{33})}{3(M_4^2 - 4M_4M_{43} - 3M_{43}^2)}. \tag{29}$$

For physically meaningful solutions, we need to check the sign of the right hand side of Eqs. (28) and (29), which should be positive. Taking the positive square root of the positive x as the value of ω, and after substituting into the expressions for M_3, M_4, M_{33} and M_{43}, we obtain the right hand side of Eqs. (28) and (29). Since each frequency root corresponds to two amplitude values for the first and third harmonic pitch motion, and the left hand side of Eqs. (28) and (29) is the amplitude squared, only those roots that give positive amplitudes are retained. For the cases we considered, there is only one frequency that satisfies all these conditions, and hence it is taken to be the physically meaningful solution. As in the first harmonic balance method, we take the first harmonic pitch motion as reference and obtain the phase relation for the third harmonic pitch and plunge motions as

$$\phi_3 = \arctan(b_3/a_3), \quad \varphi_1 = \arctan(f_1/e_1), \quad \varphi_3 = \arctan(f_3/e_3). \tag{30}$$

2.3. An improved first harmonic balance method

The higher harmonic balance method that retains terms of 3ω is rather complex algebraically. A simpler method giving some improvement to the first harmonic balance method can be obtained using the idea of Popov [12] when the coefficients of the higher harmonics are small and we assume the motion to be of the form

$$\alpha(\tau) = a_1 \sin\omega\tau + \varepsilon\vartheta(\tau), \quad \xi(\tau) = e_1 \sin\omega\tau + f_1 \cos\omega\tau + \varepsilon\sigma(\tau), \tag{31}$$

where

$$\vartheta(\tau) = \sum_{k=2}(a_k \sin k\omega\tau + b_k \cos k\omega\tau) = \sum_{k=2} \vartheta_k(\tau),$$
$$\sigma(\tau) = \sum_{k=2}(e_k \sin k\omega\tau + f_k \cos k\omega\tau) = \sum_{k=2} \sigma_k(\tau), \tag{32}$$

and ε is a small parameter. For a single cubic nonlinearity in the pitch dof, substituting Eq. (31) into Eqs. (7) and (12), we obtain for the ε^0 level a set of equations similar to Eq. (14), and the results of a_1, e_1, f_1, and ω are the same as that obtained for the first harmonic balance method. For the ε^1 level, we obtain for the system of a_3, b_3, e_3 and f_3:

$$\varepsilon(m_{13}a_3 + n_{13}b_3 + p_{13}e_3 + q_{13}f_3) = 0, \quad \varepsilon(m_{23}a_3 + n_{23}b_3 + p_{23}e_3 + q_{23}f_3) = 0,$$
$$\varepsilon(m_{33}a_3 + n_{33}b_3 + p_{33}e_3 + q_{33}f_3) = \tfrac{1}{4}d_{10}\beta a_1^3, \quad \varepsilon(m_{43}a_3 + n_{43}b_3 + p_{43}e_3 + q_{43}f_3) = 0 \tag{33}$$

and

$$\varepsilon a_3 = A_1/D, \quad \varepsilon b_3 = A_2/D, \quad \varepsilon e_3 = A_3/D, \quad \varepsilon f_3 = A_4/D. \tag{34}$$

The expressions for m_{i3}, n_{i3}, p_{i3}, q_{i3}, A_i ($i=1,2,3,4$) and D are given in Appendix D. For the other terms in Eq. (32), the solutions for a_k, b_k, e_k, f_k ($k=2, 4,\ldots,$) are all zero. Popov's method can be extended to give improved analytical solution for cubic nonlinearity in the plunge dof or in both dof.

3. Illustrative examples

In the following examples, the airfoil parameters used are: $\mu=100$, $r_\alpha=0.5$, $a_h=-0.5$, $\zeta_\xi=\zeta_\alpha=0$. Other properties of the airfoil, such as, $\bar{\omega}$, x_α, are varied.

3.1. Comparison of analytical methods with numerical computations

A typical example of the airfoil motion with a cubic nonlinearity in the pitch dof is given in this paper for a value of $\beta = 80$ and $\gamma = 0$. The values for x_α and $\bar{\omega}$ are 0.25 and 0.2, respectively. The results obtained from the first harmonic balance (HB1), high harmonic balance (HB3), and improved first harmonic balance (Popov) methods are shown in Fig. 2 for the pitch amplitude versus velocity ratio U^*/U_L^*. The pitch amplitude is determined from $\alpha' = 0$. In this case, the bifurcation parameter is the velocity ratio, and for U^* equal to the linear flutter speed $U_L^* = 6.2851$, a supercritical Hopf-bifurcation is detected. Limit cycle oscillations are observed by increasing U^* for values greater than U_L^*.

Comparisons are made with numerical simulations from a fourth-order Runge–Kutta time integration scheme using Eq. (12) with initial conditions set to $\alpha(0) = 1^\circ$ and $\alpha'(0) = \xi'(0) = \xi(0) = 0$. It is found that at $U^*/U_L^* \approx 2$, a jump phenomenon in the pitch amplitude is detected. The jump position depends on the initial conditions. For example, it varies from $U^*/U_L^* = 1.98$ to $U^*/U_L^* = 2.08$ for $\alpha(0)$ between 0.5° and 10° while keeping $\alpha'(0) = \xi(0) = \xi'(0) = 0$. With different combinations of $\alpha(0)$, $\alpha'(0)$, $\xi(0)$ and $\xi'(0)$ the jump position changes. A small change in the slope of the pitch amplitude versus U^*/U_L^* curve is detected at $U^*/U_L^* \approx 2$ for the first harmonic pitch motion as shown in Fig. 2. However, there is a large increase in the amplitude of the third harmonic indicating the importance of this harmonic after the jump. Fig. 2 also shows that the accuracy of the pitch motion for $U^*/U_L^* > 1.25$ determined by the HB1 method is rather poor compared with numerical computations. The Popov's method improves the result slightly by including a small third harmonic term, while the HB3 method gives good accuracy before the jump. For motions after the jump, the prediction from HB3 for the first harmonic agrees with the numerical results since the jump at $U^*/U_L^* \approx 2$ is very small. However, the amplitude of the third harmonic curves show that Popov's and the HB3 results are far below the numerical computations and the jump phenomenon cannot be predicted analytically.

A spectral analysis has been carried out to determine the Fourier components of the pitch and plunge motions. Fig. 3 shows a power spectral density (PSD) plot of the pitch motion obtained

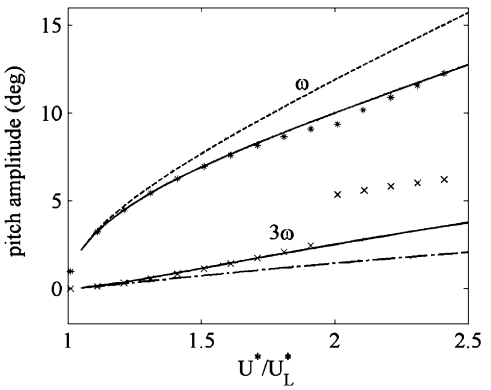

Fig. 2. Pitch amplitude versus U^*/U_L^*. Star: numerical; cross: numerical; solid line: HB3; dash line: HB1; chain-dash line: Popov's method.

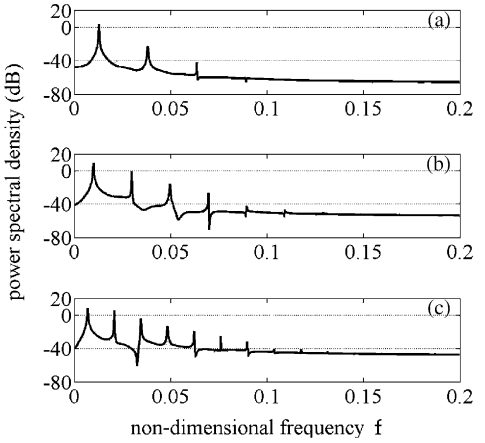

Fig. 3. Pitch motion PSD plots from numerical simulations. (a) $U^*/U_L^* = 1.2$, (b) $U^*/U_L^* = 1.98$, and (c) $U^*/U_L^* = 2.0$.

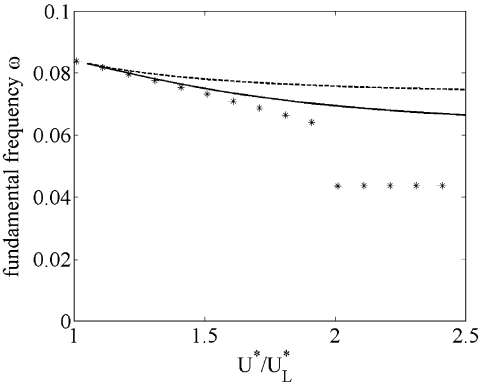

Fig. 4. Fundamental frequency versus U^*/U_L^*. Star: numerical; solid line: HB3; dash line: HB1 and Popov's method.

from numerical simulations for three values of U^*/U_L^*. Sufficiently far from the jump ($U^*/U_L^* = 1.2$), the dominant frequency is the first harmonic at $f = 0.0127$ while the third harmonic at $f = 0.0381$ is quite small (Fig. 3a). Just ahead of the jump at $U^*/U_L^* = 1.98$ (Fig. 3b), the amplitude of the third harmonic increases substantially, and the fifth and seventh harmonics are quite noticeable. The frequency f of the first harmonic decreases to 0.01. Immediately behind the jump, Fig. 3c shows at $U^*/U_L^* = 2.0$, that f decreases further to a value of 0.007, and more higher harmonics appear. The amplitude of the thirteenth harmonic becomes noticeable, although its value is small.

Fig. 4 shows the fundamental frequency ω of the pitch and plunge motions obtained numerically and analytically. The HB3 method gives an improvement over the HB1 results, and associated with the jump in amplitude, there is also a jump in frequency. Again, the jump position at $U^*/U_L^* \approx 2$ cannot be predicted from either Eqs. (16) or (27).

The phase angle (ϕ_3) of the third harmonic relative to the first harmonic as given in Eq. (30) is shown in Fig. 5. The HB3 method shows an improvement over Popov's method for $U^*/U_L^* < 2$,

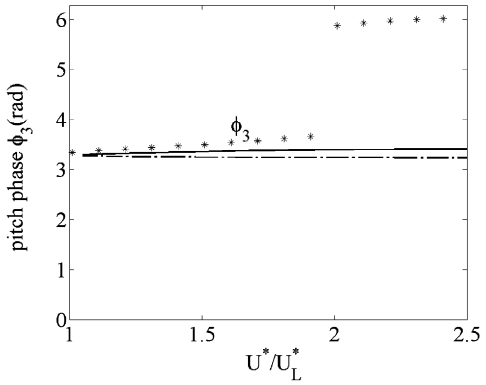

Fig. 5. Phase angle of pitch motion (third harmonic) versus U^*/U_L^*. Star: numerical; solid line: HB3; chain-dash line: Popov's method.

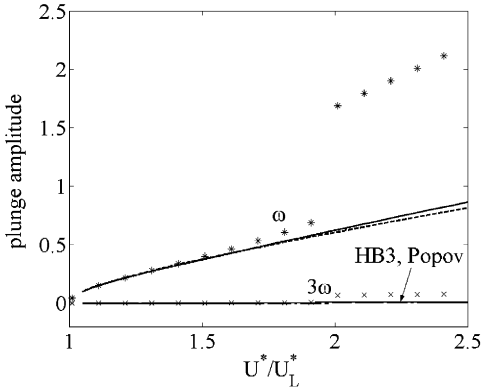

Fig. 6. Plunge amplitude versus U^*/U_L^*. Star: numerical; cross: numerical; solid line: HB3; dash line: HB1; chain-dash line: Popov's method.

and an abrupt change of approximately 2.3 radians in phase angle occurs when the amplitude jumps at $U^*/U_L^* \approx 2$. For $U^*/U_L^* > 2$, the analytical results are poor.

Fig. 6 shows that HB1, Popov's and HB3 methods give quite similar results for the plunge amplitude determined from $\xi' = 0$. Unlike the pitch motion, the jump in the amplitude of the first harmonic is large, while that for the third harmonic is small.

The phase angle of the plunge motion relative to the first harmonic pitch motion is shown in Fig. 7. For the first harmonic, HB1 and HB3 methods give almost identical results for φ_1 as given in Eqs. (21) and (30), and the two motions are practically in phase. There is some improvement in φ_3 for the third harmonic using HB3 over Popov's method for $U^*/U_L^* < 2$, but they both yield poor comparisons with numerical computations. The jump at $U^*/U_L^* \approx 2$ is about 2.1 radians and is very close to that observed for the pitch motion.

The example given here is for a value of β sufficiently large that a jump condition in amplitude is detected, and is chosen to show the limitations of the analytical methods. By a suitable scaling

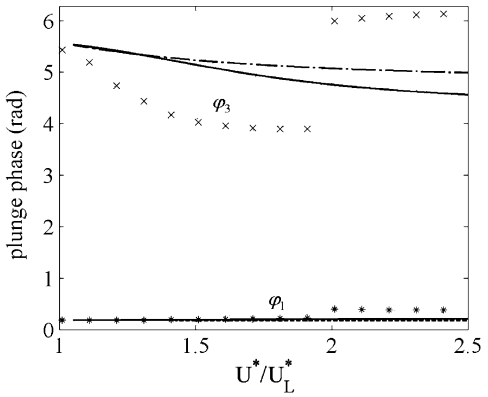

Fig. 7. Phase angle of plunge motion versus U^*/U_L^*. Star: numerical; cross: numerical; solid line: HB3; dash line: HB1; chain-dash line: Popov's method.

procedure, it can be shown that the amplitude of both pitch and plunge motions is proportional to $1/\beta^{1/2}$. For small values of β, usually the jump condition is not reached before the amplitude reaches such large values so as to invalidate the aerodynamics assumptions used in Eqs. (5) and (6). In such cases where only results with a value of U^*/U_L^* that is not significantly greater than unity are of interest, HB1 and Popov's methods give reasonably good results and they are comparable to the more algebraically complex HB3 method.

3.2. Effect of natural frequency ratio on bifurcation

In this example the spring constants are the same as those used in Section 3.1. The airfoil parameters are similar except for $x_\alpha = 0.1$ and $\bar{\omega} = 1.0, 1.2$ and 1.4. The linear flutter velocities for these values of $\bar{\omega}$ are 2.5611, 2.951 and 4.881, respectively. Since the interest is in the effect of $\bar{\omega}$ on the bifurcation behaviour near the linear flutter speed, the HB1 method is sufficiently accurate for this purpose.

Fig. 8 shows the peak value of the pitch and plunge amplitude determined from $\alpha' = 0$ and $\xi' = 0$, respectively, for $\bar{\omega} = 1.0$. A supercritical Hopf-bifurcation occurs at $U^*/U_L^* = 1$. The numerical simulations are obtained from a fourth-order Runge–Kutta time integration scheme using Eq. (12) with initial conditions set to $\alpha(0) = 1^\circ$ and $\alpha'(0) = \xi(0) = \xi'(0) = 0$. The comparison between the HB1 method and numerical computations is extremely good up to $U^*/U_L^* = 1.5$. The HB3 results are very close to those for HB1 and they are indistinguishable when plotted on the same graph. This is also the case for Figs. 9 and 12 to be shown later.

Increasing $\bar{\omega}$ to 1.2 the analytical method shows a subcritical Hopf-bifurcation. The HB1 method gives three solutions for each value of U^*/U_L^*. One of the solutions lies on the middle unstable branch in Fig. 9. The other two solutions can either have zero amplitude on the lower branch that coincides with the U^*/U_L^* axis or it can be located on the upper branch with finite amplitude. For this set of initial conditions, the numerical computations give a solution with zero amplitude in the pitch and plunge motion for $0.95 \leqslant U^*/U_L^* \leqslant 1.0$. In the range $1.0 \leqslant U^*/U_L^* \leqslant 1.159$, the amplitude variation with time is large for a given value of U^*/U_L^*.

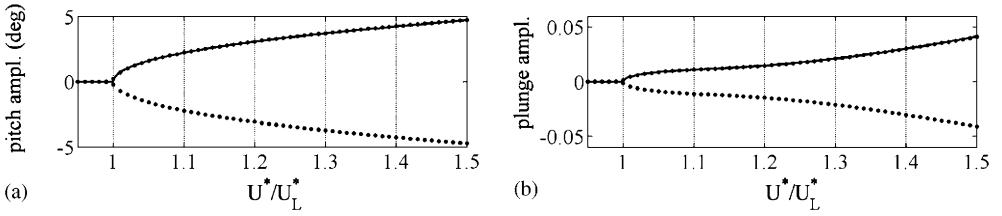

Fig. 8. (a) Pitch, and (b) plunge amplitude versus U^*/U_L^* at $\bar{\omega}=1.0$. Dot: numerical; solid line: HB1/HB3.

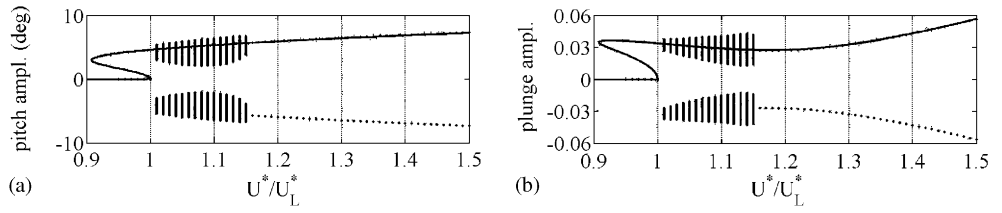

Fig. 9. (a) Pitch, and (b) plunge amplitude versus U^*/U_L^* at $\bar{\omega}=1.2$. Dot: numerical; solid line: HB1/HB3.

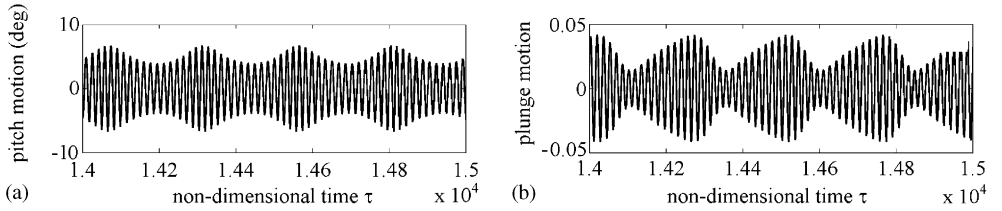

Fig. 10. Time series for (a) pitch, and (b) plunge motion at $\bar{\omega}=1.2$ and $U^*/U_L^*=1.15$.

For example, the pitch and plunge time series at $U^*/U_L^*=1.15$ are shown in Fig. 10 and they are amplitude modulated. An FFT performed on the time series shows a number of sharp peaks at discrete frequencies. In Fig. 11 an FFT of the pitch motion shown in Fig. 10 is given and the largest peak is detected at a nondimensional frequency $f_1=0.0591$. A number of smaller peaks are observed and it is found that the difference in frequency between peaks Δf lies between 0.0039 and 0.0041. Within the numerical error in reading the frequency from the FFT plot, it can be said that the frequency separation is approximately constant. The modulation frequency computed from Fig. 10 is approximately 0.004 which agrees with Δf from the FFT. The frequency of the pitch motion determined from Fig. 10 is approximately 0.059 which corresponds to f_1 in Fig. 11. For $U^*/U_L^*\geqslant 1.159$, HB1 results in Fig. 9 agree with numerical computations extremely well. The nature of the time series observed from numerical simulations in the range $1\leqslant U^*/U_L^*\leqslant 1.159$ is not fully understood and this phenomenon is presently under investigation. Similar results are obtained for the plunge motion.

A perturbation-incremental method developed by Chung et al. [13] for the investigation of strongly nonlinear autonomous oscillators with many dof is applied to this problem. It is found

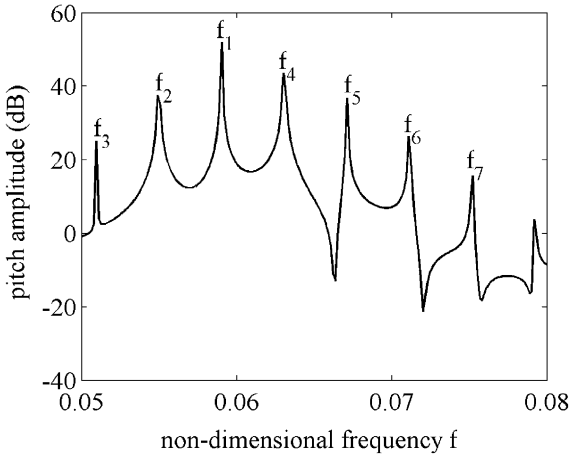

Fig. 11. FFT of pitch motion at $\bar{\omega} = 1.2$ and $U^*/U_L^* = 1.15$. $f_1 = 0.0591$, $f_2 = 0.0549$, $f_3 = 0.0510$, $f_4 = 0.0630$, $f_5 = 0.0671$, $f_6 = 0.0711$, $f_7 = 0.0752$.

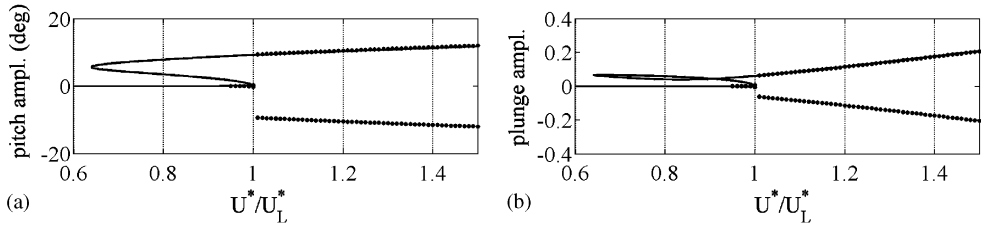

Fig. 12. (a) Pitch, and (b) plunge amplitude versus U^*/U_L^* at $\bar{\omega} = 1.4$. Dot: numerical; solid line: HB1/HB3.

that a saddle-node bifurcation occurs at $U^*/U_L^* = 0.9084$ where a Floquet multiplier crosses the unit circle at 1. The upper branch in Fig. 9 for $0.9084 \leqslant U^*/U_L^* \leqslant 0.9643$ is stable and a limit cycle emerges. Between $0.9643 \leqslant U^*/U_L^* \leqslant 1.1508$, a torus bifurcation occurs in which a pair of Floquet multipliers crosses the unit circle at points other than ± 1, and the stable solutions are tori. Limit cycle becomes stable again for $U^*/U_L^* > 1.1508$. The U^*/U_L^* range where stable torus occurs is very close to that predicted numerically.

A further increase of $\bar{\omega}$ to 1.4, both HB1, HB3 and numerical simulations predict a stable limit cycle for $U^*/U_L^* > 1.0$. The amplitude of the pitch and plunge motion determined from $\alpha' = 0$ and $\xi' = 0$, respectively, agrees almost perfectly between HB1, HB3 and numerical simulations as shown in Fig. 12. On the other hand, by using the perturbation-incremental method we obtain further that the upper branch of the pitch bifurcation diagram between $0.6409 \leqslant U^*/U_L^* \leqslant 0.8334$ is unstable, but the limit cycle becomes stable for $U^*/U_L^* > 0.8334$. Using the initial conditions set at $\alpha(0) = 1^\circ$ and $\alpha'(0) = \xi(0) = \xi'(0) = 0$, solutions are only obtained on the lower branch between $0.95 \leqslant U^*/U_L^* \leqslant 1.0$, and on the upper branch for $U^*/U_L^* > 1.0$. The upper stable branch in the pitch motion bifurcation diagram for $U^*/U_L^* > 0.8334$ can be reached by using different initial conditions in the time integration scheme. For example, Fig. 13 shows the numerical solution of

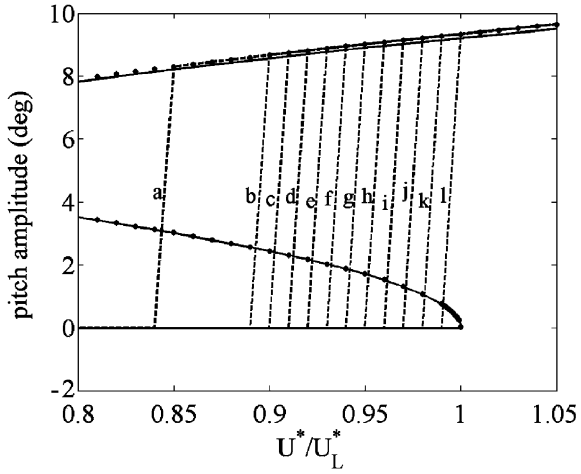

Fig. 13. Effect of $\alpha(0)$ on pitch motion subcritical Hopf-bifurcation location at $\bar{\omega} = 1.4$, $\alpha'(0) = \xi(0) = \xi'(0) = 0$. Solid line: HB1; dot: HB3; dash line: numerical. Each dash line corresponds to the following initial conditions: (a) $\alpha(0) = 12.0^{\circ}$; (b) $\alpha(0) = 10.0^{\circ}$; (c) $\alpha(0) = 8.0^{\circ}, 8.5^{\circ}, 9.0^{\circ}, 9.5^{\circ}$; (d) $\alpha(0) = 7.0^{\circ}, 7.5^{\circ}$; (e) $\alpha(0) = 6.5^{\circ}$; (f) $\alpha(0) = 6.0^{\circ}$; (g) $\alpha(0) = 5.5^{\circ}$; (h) $\alpha(0) = 5.0^{\circ}$; (i) $\alpha(0) = 4.5^{\circ}$; (j) $\alpha(0) = 4.0^{\circ}$; (k) $\alpha(0) = 3.0^{\circ}, 3.5^{\circ}$; (l) $\alpha(0) = 0.5^{\circ}, 1.0^{\circ}, 1.5^{\circ}, 2.0^{\circ}, 2.5^{\circ}$.

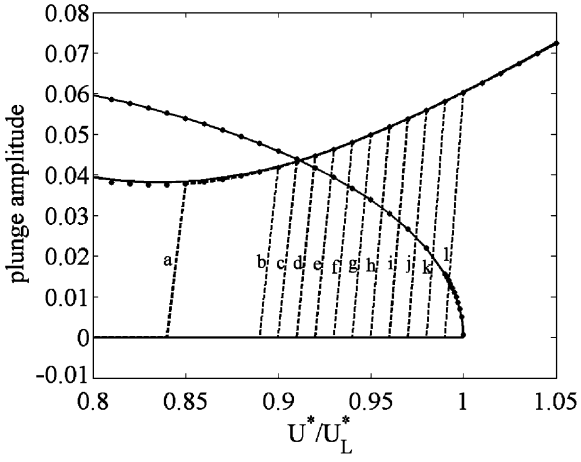

Fig. 14. Effect of $\alpha(0)$ on plunge motion subcritical Hopf-bifurcation location at $\bar{\omega} = 1.4$, $\alpha'(0) = \xi(0) = \xi'(0) = 0$. Identification of curves is similar to Fig. 13.

the pitch amplitude determined from $\alpha' = 0$ for different values of $\alpha(0)$ while setting $\alpha'(0) = \xi(0) = \xi'(0) = 0$. Also shown in the figure are the HB1 and HB3 results. The HB1 results are almost identical to those from HB3 except on the upper branch where a small difference is seen. On this branch HB3 agrees perfectly with numerical simulations. With different combinations of these four initial conditions, the jump between the stable branches can occur for $U^*/U_L^* \geqslant 0.8334$. The cross over between the stable and unstable branches for the plunge motion shown in Fig. 12 is an interesting phenomenon that is still under investigation. Again, by

varying $\alpha(0)$ while setting $\alpha'(0)=\xi(0)=\xi'(0)=0$, a figure similar to Fig. 13 can be obtained for the plunge motion. Fig. 14 shows only a few jump points between the two stable branches in the bifurcation diagram. By continuing the upper branch from $U^*/U_L^*=0.91$ to 0.8334, it is seen that the unstable branch lies above the stable branch. However, a jump between the two stable branches is possible numerically. The HB1 and HB3 give almost identical results for the plunge motion.

4. Concluding remarks

The harmonic balance method applied to the pitch/plunge motion of an airfoil with a cubic nonlinearity in the restoring forces is formulated in a manner that the frequency and amplitude can be determined directly by solving a nonlinear algebraic equation without an iteration procedure commonly used by the aeroelastician. A higher order solution is also presented which is algebraically more complex. The results obtained can be in very good agreement with those obtained from numerical simulations for certain airfoil motions. Two examples are given when the harmonic balance method fails to predict some interesting phenomena that can only be simulated numerically, that being a secondary bifurcation. However, by including terms at least up to the ninth harmonic in the series representation for the pitch and plunge motions, the dynamics of the secondary bifurcation can be captured for the airfoil parameters investigated in [14].

Appendix A. Coefficients in aeroelastic equations (Eq. (12))

$$
\begin{aligned}
&c_0 = 1 + 1/\mu,\ \ c_1 = x_\alpha - a_h/\mu,\ \ c_2 = 2(1-\psi_1-\psi_2)/\mu + 2\varsigma_\xi\bar{\omega}/U^*,\\
&c_3 = (1+(1-2a_h)(1-\psi_1-\psi_2))/\mu,\quad c_4 = 2(\varepsilon_1\psi_1+\varepsilon_2\psi_2)/\mu,\\
&c_5 = 2(1-\psi_1-\psi_2+(1/2-a_h)(\varepsilon_1\psi_1+\varepsilon_2\psi_2))/\mu,\\
&c_6 = 2\varepsilon_1\psi_1(1-\varepsilon_1(1/2-a_h))/\mu,\quad c_7 = 2\varepsilon_2\psi_2(1-\varepsilon_2(1/2-a_h))/\mu,\quad c_8 = -2\varepsilon_1^2\psi_1/\mu,\\
&c_9 = -2\varepsilon_2^2\psi_2/\mu,\quad c_{10} = \left(\bar{\omega}/U^*\right)^2,\quad d_0 = x_\alpha/r_\alpha^2 - a_h/\mu r_\alpha^2,\quad d_1 = 1+\left(1+8a_h^2\right)/8\mu r_\alpha^2,\\
&d_2 = -(1+2a_h)(1-\psi_1-\psi_2)/\mu r_\alpha^2,\\
&d_3 = (1-2a_h)/2\mu r_\alpha^2 - (1+2a_h)(1-2a_h)(1-\psi_1-\psi_2)/2\mu r_\alpha^2 + 2\varsigma_\alpha/U^*,\\
&d_4 = -(1+2a_h)(\varepsilon_1\psi_1+\varepsilon_2\psi_2)/\mu r_\alpha^2,\\
&d_5 = -(1+2a_h)(1-\psi_1-\psi_2)/\mu r_\alpha^2 - (1+2a_h)(1-2a_h)(\psi_1\varepsilon_1-\psi_2\varepsilon_2)/2\mu r_\alpha^2,\\
&d_6 = -(1+2a_h)\psi_1\varepsilon_1(1-\varepsilon_1(1/2-a_h))/\mu r_\alpha^2,\\
&d_7 = -(1+2a_h)\psi_2\varepsilon_2(1-\varepsilon_2(1/2-a_h))/\mu r_\alpha^2,\\
&d_8 = (1+2a_h)\psi_1\varepsilon_1^2/\mu r_\alpha^2,\\
&d_9 = (1+2a_h)\psi_2\varepsilon_2^2/\mu r_\alpha^2, d_{10} = \left(1/U^*\right)^2.
\end{aligned}
$$

Appendix B. Coefficients in amplitude–frequency relations (Eq. (14))

$$t_1 = \left(\varepsilon_1^2 + \omega^2\right)^{-1}, \quad t_2 = \left(\varepsilon_2^2 + \omega^2\right)^{-1}, \quad m_1 = -c_1\omega^2 + c_5 + c_6\varepsilon_1 t_1 + c_7\varepsilon_2 t_2,$$
$$m_2 = c_3\omega - c_6\omega t_1 - c_7\omega t_2, \quad m_3 = -d_1\omega^2 + d_5 + d_6\varepsilon_1 t_1 + d_7\varepsilon_2 t_2 + d_{10},$$
$$m_4 = d_3\omega - d_6\omega t_1 - d_7\omega t_2, \quad p_1 = -c_0\omega^2 + c_4 + c_8\varepsilon_1 t_1 + c_9\varepsilon_2 t_2 + c_{10},$$
$$p_2 = c_2\omega - c_8\omega t_1 - c_9\omega t_2, \quad p_3 = -d_0\omega^2 + d_4 + d_8\varepsilon_1 t_1 + d_9\varepsilon_2 t_2,$$
$$p_4 = d_2\omega - d_8\omega t_1 - d_9\omega t_2, \quad q_1 = -p_2, \quad q_2 = p_1, \quad q_3 = -p_4, \quad q_4 = p_3,$$
$$E_1 = -\frac{m_1 p_1 + m_2 p_2}{p_1^2 + p_2^2}, \quad F_1 = \frac{m_1 p_2 - m_2 p_1}{p_1^2 + p_2^2}.$$

Appendix C. Coefficients in frequency relation (Eq. (16))

$$l_0 = c_2(d_4 - d_0 x) - d_2(c_4 - c_0 x + c_{10}), \quad l_1 = c_2 d_8\varepsilon_1 - d_2 c_8\varepsilon_1 - c_8(d_4 - d_1 x) + d_8(c_4 - c_0 x + c_{10}),$$
$$l_2 = c_2 d_9\varepsilon_2 - d_2 c_9\varepsilon_2 - c_9(d_4 - d_0 x) + d_9(c_4 - c_0 x + c_{10}), \quad l_3 = (\varepsilon_1 - \varepsilon_2)(c_8 d_9 - c_9 d_8),$$
$$g_0 = l_0(c_5 - c_1 x), \quad g_1 = l_1(c_5 - c_1 x) + l_0 c_6\varepsilon_1, \quad g_2 = l_2(c_5 - c_1 x) + l_0 c_7\varepsilon_2,$$
$$g_3 = l_1 c_6\varepsilon_1, \quad g_4 = l_2 c_7\varepsilon_2, \quad g_5 = l_3(c_5 - c_1 x) + l_1 c_7\varepsilon_2 + l_2 c_6\varepsilon_1, \quad g_6 = g_7 = 0, \quad g_8 = l_3 c_6\varepsilon_1,$$
$$g_9 = l_3 c_7\varepsilon_2, \quad h_0 = (c_4 - c_0 x + c_{10})(d_4 - d_0 x) + c_2 d_2 x,$$
$$h_1 = (c_4 - c_0 x + c_{10}) d_8\varepsilon_1 + (d_4 - d_0 x) c_8\varepsilon_1 - c_2 d_8 x - c_8 d_2 x,$$
$$h_2 = (c_4 - c_0 x + c_{10}) d_9\varepsilon_2 + (d_4 - d_0 x) c_9\varepsilon_2 - c_2 d_9 x - c_9 d_2 x, \quad h_3 = c_8 d_8(\varepsilon_1^2 + x),$$
$$h_4 = c_9 d_9(\varepsilon_2^2 + x), \quad h_5 = (c_9 d_8 + c_8 d_9)(x + \varepsilon_1\varepsilon_2),$$
$$k_0 = c_3 h_0, \quad k_1 = c_3 h_1 - c_6 h_0, \quad k_2 = c_3 h_2 - c_7 h_0, \quad k_3 = c_3 h_3 - c_6 h_1, \quad k_4 = c_3 h_4 - c_7 h_2,$$
$$k_5 = c_3 h_5 - c_7 h_1 - c_6 h_2, \quad k_6 = -c_6 h_3, \quad k_7 = -c_7 h_4, \quad k_8 = -c_6 h_5 - c_7 h_3, \quad k_9 = -c_6 h_4 - c_7 h_5,$$
$$u_0 = (c_4 - c_0 x + c_{10})^2 + c_2^2 x, \quad u_1 = 2(c_4 - c_0 x + c_{10}) c_8\varepsilon_1 - 2 c_2 c_8 x,$$
$$u_2 = 2(c_4 - c_0 x + c_{10}) c_9\varepsilon_2 - 2 c_2 c_9 x, \quad u_3 = c_8^2(\varepsilon_1^2 + x), \quad u_4 = c_9^2(\varepsilon_2^2 + x), \quad u_5 = 2 c_8 c_9(\varepsilon_1\varepsilon_2 + x),$$
$$v_0 = d_3 u_0, \quad v_1 = d_3 u_1 - d_6 u_0, \quad v_2 = d_3 u_2 - d_7 u_0, \quad v_3 = d_3 u_3 - d_6 u_1, \quad v_4 = d_3 u_4 - d_7 u_2,$$
$$v_5 = d_3 u_5 - d_7 u_1 - d_6 u_2, \quad v_6 = -d_6 u_3, \quad v_7 = -d_7 u_4, \quad v_8 = -d_6 u_5 - d_7 u_3, \quad v_9 = -d_6 u_4 - d_7 u_5.$$
$$L_i = g_i - k_i + v_i \quad (i = 0, 1, 2, ..., 9).$$

Appendix D. Coefficients in third harmonic balance method (Eq. (24))

$$t_{13} = \left(\varepsilon_1^2 + (3\omega)^2\right)^{-1}, \quad t_{23} = \left(\varepsilon_2^2 + (3\omega)^2\right)^{-1}, \quad m_{13} = -c_1 9\omega^2 + c_5 + c_6\varepsilon_1 t_{13} + c_7\varepsilon_2 t_{23},$$
$$m_{23} = c_3 3\omega - c_6 3\omega t_{13} - c_7 3\omega t_{23}, \quad m_{33} = -d_1 9\omega^2 + d_5 + d_6\varepsilon_1 t_{13} + d_7\varepsilon_2 t_{23} + d_{10},$$
$$m_{43} = d_3 3\omega - d_6 3\omega t_{13} - d_7 3\omega t_{23}, \quad n_{13} = -m_{23}, \quad n_{23} = m_{13}, \quad n_{33} = -m_{43}, \quad n_{43} = m_{33},$$
$$p_{13} = -c_0 9\omega^2 + c_4 + c_8\varepsilon_1 t_{13} + c_9\varepsilon_2 t_{23} + c_{10}, \quad p_{23} = c_2 3\omega - c_8 3\omega t_{13} - c_9 3\omega t_{23},$$
$$p_{33} = -d_0 9\omega^2 + d_4 + d_8\varepsilon_1 t_{13} + d_9\varepsilon_2 t_{23}, \quad p_{43} = d_2 3\omega - d_8 3\omega t_{13} - d_9 3\omega t_{23},$$
$$q_{13} = -p_{23}, \quad q_{23} = p_{13}, \quad q_{33} = -p_{43}, \quad q_{43} = p_{33};$$

$$
\begin{aligned}
D = {} & m_{13}(n_{23}(p_{33}q_{43} - q_{33}p_{43}) - n_{33}(p_{23}q_{43} - q_{23}p_{43}) + n_{43}(p_{23}q_{33} - q_{23}p_{33})) \\
& - m_{23}(n_{13}(p_{33}q_{43} - q_{33}p_{43}) - n_{33}(p_{13}q_{43} - q_{13}p_{43}) + n_{43}(p_{13}q_{33} - q_{13}p_{33})) \\
& + m_{33}(n_{13}(p_{23}q_{43} - q_{23}p_{43}) - n_{23}(p_{13}q_{43} - q_{13}p_{43}) + n_{43}(p_{13}q_{23} - q_{13}p_{23})) \\
& - m_{43}(n_{13}(p_{23}q_{33} - q_{23}p_{33}) - n_{23}(p_{13}q_{33} - q_{13}p_{33}) + n_{33}(p_{13}q_{23} - q_{13}p_{23})),
\end{aligned}
$$

$$
\begin{aligned}
A_1 &= \tfrac{1}{4}d_{10}\beta a_1^3(n_{13}(p_{23}q_{43} - q_{23}p_{43}) - n_{23}(p_{13}q_{43} - q_{13}p_{43}) + n_{43}(p_{13}q_{23} - q_{13}p_{23})), \\
A_2 &= -\tfrac{1}{4}d_{10}\beta a_1^3(m_{13}(p_{23}q_{43} - q_{23}p_{43}) - m_{23}(p_{13}q_{43} - q_{13}p_{43}) + m_{43}(p_{13}q_{23} - q_{13}p_{23})), \\
A_3 &= \tfrac{1}{4}d_{10}\beta a_1^3(m_{13}(n_{23}q_{43} - q_{23}n_{43}) - m_{23}(n_{13}q_{43} - q_{13}n_{43}) + m_{43}(n_{13}q_{23} - q_{13}n_{23})), \\
A_4 &= -\tfrac{1}{4}d_{10}\beta a_1^3(m_{13}(n_{23}p_{43} - p_{23}n_{43}) - m_{23}(n_{13}p_{43} - p_{23}n_{43}) + m_{43}(n_{13}p_{23} - p_{13}n_{23})),
\end{aligned}
$$

$$
E_3 = -\frac{m_{13}p_{13} + m_{23}p_{23}}{p_{13}^2 + p_{23}^2}, \quad F_3 = \frac{m_{13}p_{23} - m_{23}p_{13}}{p_{13}^2 + p_{23}^2}, \quad M_3 = \frac{1}{(p_1q_2 - p_2q_1)}\begin{vmatrix} m_1 & p_1 & q_1 \\ m_2 & p_2 & q_2 \\ m_3 & p_3 & q_3 \end{vmatrix},
$$

$$
M_4 = \frac{1}{(p_1q_2 - p_2q_1)}\begin{vmatrix} m_1 & p_1 & q_1 \\ m_2 & p_2 & q_2 \\ m_4 & p_4 & q_4 \end{vmatrix}, \quad M_{33} = \frac{1}{(p_{13}q_{23} - p_{23}q_{13})}\begin{vmatrix} m_{13} & p_{13} & q_{13} \\ m_{23} & p_{23} & q_{23} \\ m_{33} & p_{33} & q_{33} \end{vmatrix},
$$

$$
M_{43} = \frac{1}{(p_{13}q_{23} - p_{23}q_{13})}\begin{vmatrix} m_{13} & p_{13} & q_{13} \\ m_{23} & p_{23} & q_{23} \\ m_{43} & p_{43} & q_{43} \end{vmatrix}, \quad N_{33} = \frac{1}{(p_{13}q_{23} - p_{23}q_{13})}\begin{vmatrix} n_{13} & p_{13} & q_{13} \\ n_{23} & p_{23} & q_{23} \\ n_{33} & p_{33} & q_{33} \end{vmatrix},
$$

$$
N_{43} = \frac{1}{(p_{13}q_{23} - p_{23}q_{13})}\begin{vmatrix} n_{13} & p_{13} & q_{13} \\ n_{23} & p_{23} & q_{23} \\ n_{43} & p_{43} & q_{43} \end{vmatrix}.
$$

References

[1] D.S. Woolston, H.L. Runyan, R.E. Andrews, An investigation of effects of certain types of structural nonlinearities on wing and control surface flutter, *Journal Aeronautical Sciences* 24 (1) (1957) 57–63.

[2] S.F. Shen, An approximate analysis of nonlinear flutter problems, *Journal Aeronautical Sciences* 26 (1) (1959) 25–32.

[3] B.H.K. Lee, P. LeBlanc, Flutter analysis of a two-dimensional airfoil with cubic nonlinear restoring force, NAE-AN-36, National Research Council, Canada, 1986.

[4] B.H.K. Lee, L.Y. Jiang, Y.S. Wong, Flutter of an airfoil with a cubic restoring force, *Journal of Fluids and Structures* 13 (1) (1999) 75–101.

[5] L. Liu, Y.S. Wong, B.H.K. Lee, Application of the centre manifold theory in nonlinear aeroelasticity, *Journal of Sound and Vibration* 234 (4) (2000) 641–659.

[6] T. O'Neil, T.W. Stragnac, Aeroelastic response of a rigid wing supported by nonlinear springs, *Journal of Aircraft* 35 (4) (1998) 616–622.

[7] B.H.K. Lee, S.J. Price, Y.S. Wong, Nonlinear aeroelastic analysis of airfoils: bifurcation and chaos, *Progress in Aerospace Sciences* 35 (1999) 205–334.
[8] J.P. Thomas, E.H. Dowell, K.C. Hall, Nonlinear inviscid aerodynamic effects on transonic divergence, flutter, and limit-cycle oscillations, *AIAA Journal* 40 (4) (2002) 638–646.
[9] Y.C. Fung, *An Introduction to the Theory of Aeroelasticity*, Dover, New York, 1993.
[10] R.T. Jones, The unsteady lift of a wing of finite aspect ratio, NACA Report 681, 1940.
[11] M.B. Monagan, K.O. Geddes, K.M. Heal, G. Lebahn, J. Vorkoetter, J. McCarron, *Maple 6 Programming Guide*, Waterloo Maple Inc., Waterloo, 2000.
[12] E.P. Popov, On the use of the harmonic linearization method in automatic control theory, NACA TM 1406, 1957.
[13] K.W. Chung, C.L. Chan, Z. Xu, G.M. Mahmoud, A perturbation-incremental method for strongly nonlinear oscillators with many degrees of freedom, *Nonlinear Dynamics* 28 (3) (2002) 243–259.
[14] L. Liu, E.H. Dowell, *The secondary bifurcation of an aeroelastic airfoil motion: effect of high harmonics. Nonlinear Dynamics* 37 (1) (2004) 31–49.